Life Sciences 234 (2019) 116770

Contents lists available at ScienceDirect

Life Sciences

journal homepage: www.elsevier.com/locate/lifescie

In vitro investigation of permeability and metabolism of licoricidin

Lina Shan[a], Gang Zhang[b], Zhe Guo[a], Xianbao Shi[a,*]

[a] The First Affiliated Hospital of Jinzhou Medical University, Jinzhou 121001, China
[b] State Key Laboratory of Bioactive Substances and Function of Natural Medicine, Institute of Materia Medica, Peking Union Medical College and Chinese Academy of Medical Sciences, Beijing 100000, China

ARTICLE INFO

Keywords:
Licoricidin
Cytochrome P450
UDP-glucuronosyltransferase
Herb-drug interactions
Permeability

ABSTRACT

Aim

Licoricidin has multiple pharmacological activities. The present study was designed to investigate the permeability and pharmacokinetic behavior of licoricidin using in vitro models.

Material and methods: First, human liver microsomes and recombinant human supersomes were used to investigate the interactions between metabolic enzymes and licoricidin. In addition, rat, minipig, rabbit, dog, monkey, and human liver microsomes were used to determine metabolic differences among species. The parallel artificial membrane permeability assay (PAMPA) was used to explore licoricidin permeability behavior.

Key findings: At 100 μM, licoricidin strongly inhibited CYP2C9, CYP2C19, CYP3A4, UGT1A3, UGT1A6, UGT1A7, UGT1A8, UGT1A9, UGT2B4, UGT2B7, UGT2B15, and UGT2B17. Licoricidin metabolism exhibited considerable differences among species; dog, pig, and rat liver microsomes showed higher metabolic capacity than the other species. Seven licoricidin metabolites were identified by liquid chromatography-tandem mass spectrometry, and hydration and hydroxylation were the major metabolic pathways. The PAMPA permeability of licoricidin was moderate at both pH 4.0 and 7.4.

Significance: The present study will support further pharmacological or toxicological research on licoricidin.

1. Introduction

At present, plants have been extensively studied [1,2]. Licorice (Glycyrrhiza species) is one of the oldest medicinal plants used in China and Far Eastern countries. Licorice root has considerable antiviral, anti-inflammatory, anticarcinogenic, antiallergy, hepatoprotective, and estrogenic activities [3,4]. In China, licorice is usually used together with other plants as an expectorant and analgesic to treat asthma, and alleviate abscesses and abdominal pain [5]. To evaluate the therapeutic potential and understand the mechanisms of action of licorice better, further research on the predominant components of licorice is required. Licoricidin, an isoflavan with two isoprenyl groups, is a major component of licorice extract, and the structure of licoricidin is shown in Fig. 1. Similar to licorice, licoricidin shows potent antibacterial [6,7], anticancer [4,8], and anti-inflammatory [5] activities. In addition, licoricidin prevents UVA-induced photoaging of human dermal fibroblasts [9].

Cytochrome P450 (CYP) and UDP-glucuronosyltransferase (UGT) are the main phase I and II enzymes, respectively, that are responsible for the biotransformation of most drugs and other hydrophilic xenobiotics [10,11]. Thus, induction or inhibition of CYPs or UGTs will alter drug pharmacokinetics and may decrease the pharmacological efficacy or increase the toxicity of drugs. The extracts of three botanically identified licorice species (*Glycyrrhiza glabra* L., *Glycyrrhiza uralensis* Fish. ex DC., and *Glycyrrhiza inflata* Batalin) strongly inhibited CYP2A1, CYP2B6, CYP2C8, CYP2C9, CYP2C19, CYP3A4, and UGT1A1 and induced CYP1A2 and CYP2B6 [12,13]. An activity loss of > 50% was observed when CYP3A4 in the reconstituted system was incubated with 6.9 g/mL of licorice root extract for 15 min in the presence of NADPH, whereas no inhibition was seen initially. The remnant activities of CYP2C8 and CYP2C9 inhibited by licoricidin (10 μM) were < 10% [3]. However, the kinetic parameters, including the half-maximal inhibitory concentration (IC_{50}) and inhibitor constant (K_i), have never been reported. Thus, it is important to validate the effect of licoricidin on the activities of CYPs and UGTs to help avoid adverse drug reactions from HDIs. In addition, it is necessary to identify the enzyme(s) involved in licoricidin biotransformation during the adverse reaction to avoid licoricidin competing with other drugs that are metabolized by the same enzyme. If licoricidin is co-administered with a drug that shares the same metabolic enzyme, the two compounds will compete with each other for the metabolic enzyme and affect blood concentrations, which may result in adverse reactions.

* Corresponding author at: The First Affiliated Hospital of Jinzhou Medical University, Jinzhou, Liaoning Province, China.
E-mail address: sxbsln@163.com (X. Shi).

https://doi.org/10.1016/j.lfs.2019.116770
Received 28 June 2019; Received in revised form 4 August 2019; Accepted 13 August 2019
Available online 14 August 2019

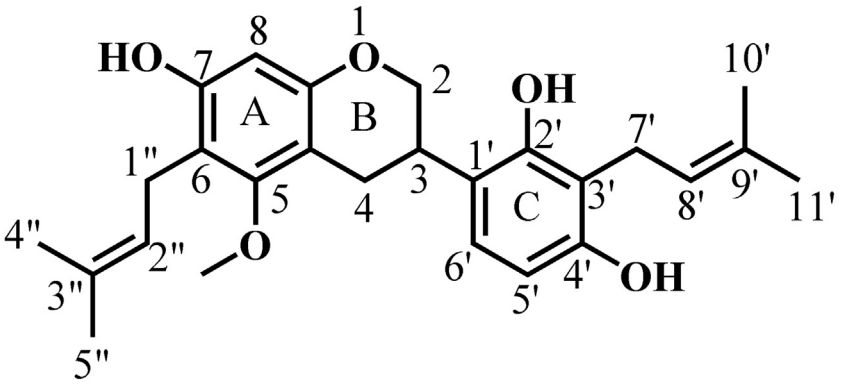

Fig. 1. Structure of licoricidin.

Numerous studies have demonstrated the biological and pharmacological activities of licoricidin. However, there has been little research on the metabolism of licoricidin. Interspecies comparison of metabolic pathways can reveal species with pathways similar to that of humans that may be suitable for future in vivo studies [14]. Thus, it is important to investigate the metabolic profiles of licoricidin and their differences among species.

The parallel artificial membrane permeability assay (PAMPA) is currently used as a rapid in vitro assay of passive biomembrane permeation in drug discovery [15]. The PAMPA in vitro technique was developed by Kansy et al. in 1998 [16] and was originally used to predict passive permeability through the gastrointestinal tract rapidly [17].

In this study, we explored the inhibition of licoricidin against 11 UGT and eight CYP isoforms, and we compared the metabolic characteristics and differences of licoricidin among six species. PAMPA was used to investigate licoricidin permeability at pH 4.0 and 7.0.

2. Materials and methods

2.1. Chemicals and reagents

Licoricidin (> 98%) was purchased from Sichuan Weikeqi Biotechnology Co., Ltd. (Sichuan, China). We have described the probe substrates, probe substrate metabolites, and positive inhibitors of CYP isoforms in our previous paper [10]. Naproxen, furosemide, 1-aminobenzotriazole (ABT), phenacetin, sulfaphenazole, chlorzoxazone, quinidine, clomethiazole, furafylline, diclofenac, dextromethorphan, ketoconazole, testosterone, (*S*)-mephenytoin, omeprazole, glucose-6-phosphate dehydrogenase, $NADP^+$, D-glucose-6-phosphate, 4-methylumbelliferone (4-MU), 4-methylumbelliferone-β-D-glucuronide, Tris–HCl, 7-hydroxycoumarin, and uridine 5′-diphosphoglucuronic acid (UDPGA; trisodium salt) were purchased from Sigma Aldrich (St. Louis, MO, USA). Metabolites of the probe substrates, which were O-deethylated phenacetin (CYP1A2), 4′-hydroxylated diclofenac (2C9), *O*-demethylated dextromethorphan (2D6), 6-hydroxylated chlorzoxazone (2E1), 6β-hydroxylated testosterone (3A4), and 4′-hydroxylated (*S*)-mephenytoin (2C19), were obtained from the Research Institute for Liver Disease Co., Ltd. (Shanghai, China). Acetonitrile (HPLC grade) was purchased from Merck (Darmstadt, Germany) and formic acid (HPLC grade) was purchased from Tedia (Fairfield, OH, USA). All other reagents and chemicals were of the highest grade commercially available.

2.2. Liver microsomes and recombinant human UGT and CYP isoforms

Pooled liver microsomes from humans (HLMs), monkeys (MLMs), rabbits (RAMs), rats (RLMs), dogs (DLMs), and minipigs (PLMs) were provided by the Research Institute for Liver Disease Co., Ltd. (Shanghai, China). The HLMs were prepared from 11 individual human donor livers. Research involving human subjects was performed under full compliance with government policies and the Helsinki Declaration, and informed consent was obtained from all subjects. MLMs, RAMs, RLMs, DLMs, and PLMs were prepared from 10 individual animal livers. Protein concentration was determined with a bicinchoninic acid protein assay kit [18]. Recombinant human supersomes (UGT1A1, UGT1A3, UGT1A6, UGT1A7, UGT1A8, UGT1A9, UGT1A10, UGT2B4, UGT2B7, UGT2B15, CYP1A2, CYP2C9, CYP2D6, CYP2E1, CYP3A4, and CYP2C19) were obtained from BD Gentest Corp. (Woburn, MA, USA).

2.3. Analytical instruments and conditions

A high-performance liquid chromatography (HPLC) system comprising two pumps (LC-20AB, Shimadzu, Kyoto, Japan), a column oven (CTO-20AB, Shimadzu; set to 40 °C), autosampler (SIL-20A, Shimadzu), and an ultraviolet (UV) detector (SPD-20A, Shimadzu) was used. HPLC analysis of samples was performed using a Hypersil BDS C18 column (Dalian Elite Analytical Instruments Co., Dalian, China; 4.6 × 150 mm, 5 μm). Mobile phases A and B were acetonitrile and water containing 0.1% formic acid, respectively. The flow rate was 1 mL/min with the following gradient program: 0.00 min, 50% B; 12.00 min, 50% B; 12.30 min, 95% B; 18.00 min, 95% B; 18.30 min, 50% B; 22.00 min, 50% B. Licoricidin and its metabolites were detected at 285 nm.

The analysis for licoricidin metabolites was conducted on an ultra-performance liquid chromatography (UPLC) system (Waters Corporation, Milford, MA, USA) equipped with a Q-TOF high-definition mass spectrometer (SYNAPT G2-Si, Waters). Separation of analytes was achieved with a UPLC BEH C18 column (Acquity, Waters; 2.1 × 100 mm, 1.7 μm). Mass detection was performed in negative mode from *m/z* 100 to 1000. The optimized parameters were as follows: collision gas, argon; trap collision energies, 6 V (low energy) and 20–50 V (high energy); capillary and cone voltages, 2 kV and 40 V; source and desolvation temperatures, 120 and 600 °C; and cone and desolvation gas flows, 50 and 800 L/h, respectively.

2.4. In vitro incubation systems with liver microsomes or recombinant CYP supersomes

The incubation system consisted of 0.3 mg/mL protein in liver microsomes or 15 nM protein in recombinant human supersomes, 4 mM $MgCl_2$, and 1 mM NADPH in a final volume of 200 μL of 0.1 M potassium phosphate buffer (pH 7.4). After pre-incubation at 37 °C for 3 min, the reaction was initiated by adding NADPH. Incubation time was optimized for 30 min, and then terminated by adding 200 μL ice-cold methanol to terminate the reaction. The incubation solution was centrifuged at 20,000 × *g* for 20 min at 4 °C. An aliquot of the supernatant was injected into the HPLC or *liquid chromatography-tandem mass spectrometry* (LC-MS/MS) system for analysis. All the incubation

experiments were performed in triplicate, and the data were expressed as mean ± standard deviation (SD).

2.5. Inhibitory effect of licoricidin on CYP activities in pooled HLMs

The inhibitory effects of licoricidin (100 μM) on the activities of six CYP isoforms (CYP1A2, CYP2C9, CYP2D6, CYP2E1, CYP3A4, and CYP2C19) were evaluated using HLMs. The marker reactions and probe substrates were phenacetin O-deethylation (CYP1A2), diclofenac 4′-hydroxylation (2C9), dextromethorphan *O*-demethylation (2D6), chlorzoxazone 6-hydroxylation (2E1), testosterone 6β-hydroxylation (3A4), and (*S*)-mephenytoin 4′-hydroxylation (2C19). The reaction system is described in Section 2.4. The inhibitors of individual CYPs used as positive controls have been reported previously (Fang et al., 2009), and the inhibitor concentrations were 10 μM furafylline for CYP1A2, 10 μM sulfaphenazole for CYP2C9, 20 μM omeprazole for CYP2C19, 10 μM quinidine for CYP2D6, 50 μM clomethiazole for CYP2E1, 1 μM ketoconazole for CYP3A4, and 500 mM ABT for broad CYP inhibition [19]. For CYP isoforms that were inhibited by > 90% total activity by 100 μM licoricidin, kinetic parameters IC_{50} and K_i were determined and analyzed. Dixon and Lineweaver-Burk plots were generated to determine the inhibition type. All incubations were performed in triplicate, and mean values were used for analysis.

2.6. Incubation and analysis methods for inhibition evaluation against UGTs

4-MU was used as a nonselective UGT probe substrate to investigate the inhibition potential of licoricidin for UGT isoforms. A typical incubation mixture (total volume of 200 μL) contained recombinant UGTs (final concentrations: 0.125, 0.05, 0.025, 0.05, 0.025, 0.05, 0.05, 0.25, 0.05, and 0.2 mg/mL for UGT1A1, UGT1A3, UGT1A6, UGT1A7, UGT1A8, UGT1A9, UGT1A10, UGT2B4, UGT2B7, and UGT2B15, respectively), 5 mM UDPGA, 5 mM $MgCl_2$, 50 mM Tris-HCl buffer (pH 7.4), and 4-MU in the absence or presence of different concentrations of licoricidin. The incubation concentrations of 4-MU were equal to known Michaelis constants (K_m) or substrate concentrations resulting in 50% of *maximum* velocity (V_{max}) (S_{50}) values for each UGT isoform (110, 1200, 110, 15, 750, 30, 80, 1200, 350, 250, and 2000 μM 4-MU for UGT1A1, UGT1A3, UGT1A6, UGT1A7, UGT1A8, UGT1A9, UGT1A10, UGT2B4, UGT2B7, UGT2B15, and UGT2B17, respectively). Licoricidin was dissolved in methanol and the final concentration of methanol was 0.5% (v/v). There was a 5 min pre-incubation step at 37 °C before the reaction was started by the addition of UDPGA. The optimized incubation times were 120 min for UGT1A1, UGT1A3, UGT1A10, UGT2B4, UGT2B7, and UGT2B15, and 30 min for UGT1A6, UGT1A7, UGT1A8, and UGT1A9. The reactions were quenched by adding 200 μL of acetonitrile containing 100 μM 7-hydroxycoumarin as an internal standard. The incubation mixture was then centrifuged at 20,000 × *g* for 20 min to obtain the supernatant and an aliquot of supernatant (20 μL) was analyzed by HPLC.

2.7. Screening with recombinant CYPs

Licoricidin was incubated with each of the cDNA-expressed human CYP isoforms (CYP1A2, CYP2C9, CYP2C19, CYP2D6, CYP2E1, and CYP3A4) to assess the involvement of each recombinant CYP enzyme in licoricidin metabolite formation. The incubation conditions and sample workup were the same as those described in Section 2.4. Licoricidin (10 μM) was incubated with each of the recombinant CYPs (15 nM) at 37 °C for 30 min and possible metabolites were identified by HPLC.

2.8. Chemical inhibition study

ABT, a broad-specificity CYP inactivator, was added to the incubation system to investigate whether CYPs were responsible for licoricidin metabolism in RLMs. If ABT inhibits the formation of licoricidin metabolites, it proves that CYPs catalyze the metabolic reaction of licoricidin. Furthermore, selective chemical inhibitors of CYPs were added to RLMs to confirm the CYP isoforms involved in the metabolism of licoricidin. The incubation conditions and times are described in Section 2.4.

2.9. Kinetics study

The enzyme kinetics of licoricidin metabolism in liver microsomes from four species (DLMs, RLMs, PLMs, and HLMs) were investigated. The assay conditions were optimized to ensure that the formation of the metabolites was linear with respect to the concentration of protein and incubation time. Enzyme kinetics reactions for metabolite formation were performed at different licoricidin concentrations (1–200 μM). The protein concentrations in the incubation systems were 0.3 mg/mL for PLMs, DLMs, RLMs, and HLMs. The other conditions were the same as those described in Section 2.4. The K_m and V_{max} values of licoricidin were calculated according to nonlinear regression from the Michaelis-Menten equation, and the results were graphically represented on Eadie-Hofstee plots (velocity versus ratio of velocity to substrate concentration). Intrinsic clearance (CL_{int}) was defined as V_{max}/K_m. Due to the lack of available metabolite standards, the metabolites in the incubation mixtures were quantified using the standard curve for licoricidin. Kinetic constants were reported as mean ± SD.

2.10. Prediction of in vivo hepatic clearance

We used Eqs. (1)(3) to predict the in vivo hepatic clearance of licoricidin in rats, dogs, and humans [20].

$$CL_{int\ in\ vitro} = \frac{V_{max}}{K_m} \quad (1)$$

$$CL_{int\ in\ vivo} = CL_{int\ in\ vitro} \cdot SF \quad (2)$$

$$CL_H = \frac{Q_H \cdot f_u \cdot CL_{int\ in\ vivo}}{Q_H + f_u \cdot CL_{int\ in\ vivo}} \quad (3)$$

Here, the scaling factor (SF) is the milligrams of microsomal protein per gram of liver multiplied by the grams of liver weight; CL_H is hepatic clearance; f_u is the free fraction in the blood (there are no data available for licoricidin; thus, f_u was arbitrarily set to 1); and Q_H is the hepatic blood flow. We have previously used Eqs. (1)(3) to calculate morusin clearance [21]. The physiological parameters for calculating the intrinsic clearance in rats, dogs, and humans have been reported by Naritomi et al. and are as follows. For rats, dogs, and humans, the amounts of microsomal protein are 44.8, 77.9, and 48.8 mg of protein/g of liver; the liver weight per kilogram of body weight values are 40, 32, and 25.7 g; and the liver blood flows are 55.2, 30.9, and 20.7 mL/min/kg, respectively [22].

2.11. Identifying the metabolites in liver microsomes from six species

The biotransformation of licoricidin was investigated by incubating licoricidin with HLMs, DLMs, PLMs, RAMs, RLMs, and MLMs. The metabolite structures were identified by UPLC-MS/MS. A 2 μL sample was injected into a C18 column (Welch, Milford, USA; 1.7 × 100 mm, 1.7 μm) using a UPLC system (Acquity H-class, Waters). The column oven was kept at 40 °C. The mobile phase consisted of liquid chromatography (LC) grade water with 0.1% formic acid (A) and LC grade acetonitrile (B) with the following gradient profile: 0.0 min, 40% B; 10.0 min, 60% B; 11 min, 95% B; 12 min, 95% B; 13 min, 40% B; 15 min, 40% B. The mass spectrometry conditions are described in Section 2.3.

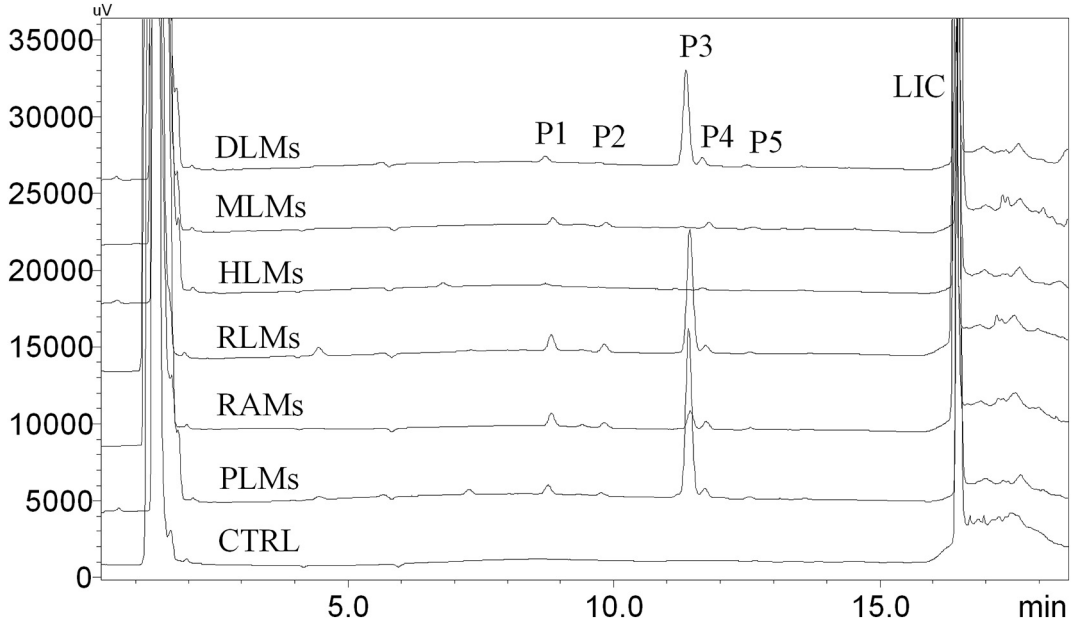

Fig. 2. Representative HPLC profiles of licoricidin and its metabolites in HLMs, DLMs, MLMs, RAMs, PLMs, and RLMs. Licoricidin (20 μM) was incubated with liver microsomes (0.3 mg/mL) at 37 °C for 30 min.

2.12. Molecular docking

Molecular docking calculates the preferred orientation of one molecule to a second when the molecules are bound to each other to form a stable complex [23]. The metabolism of compounds and metabolism-based drug-drug interactions can be predicted by molecular docking. Molecular docking of licoricidin to CYP3A4 and CYP2D6 was performed using the three-dimensional crystal structures of human CYP3A4 (PDB ID: 4K9W) and CYP2D6 (PDB ID: 4WNU) from the Protein Data Bank (http://www.rcsb.org/pdb/). Docking analysis was performed with Autodock 4.2. Discovery Studio 2017 was used for protein and ligand preparation, and the energy was minimized using the external Tripos force field. The binding modes with the lowest binding free energy and the most cluster members were chosen for the optimum docking conformation. The best docked pose of the ligand was visualized using Pymol Molecular Graphics System 0.99.

2.13. Glucuronidation assay of licoricidin in HLMs by LC-MS/MS

The 200 μL incubation mixture contained 50 mM Tris-HCl buffer (pH 7.4), 5 mM $MgCl_2$, 2 mM UDPGA, 0.1 mg/mL HLMs and 10 μM licoricidin. The reaction was initiated by the addition of UDPGA after pre-incubation at 37 °C for 3 min. After 60 min of incubation, the reaction was terminated with 200 μL of cold acetonitrile. The incubation solution was centrifuged at 20,000 × *g* for 20 min. 2 μL of the supernatant was injected into the LC-MS/MS system for analysis. Control incubations without UDPGA, substrate or microsomes were performed to confirm that the metabolite produced were microsome and UDPGA dependent.

Chromatographic separation was performed on a Shimadzu Prominence™ HPLC system with two LC-20ADXR pumps, a DGU-20A5R degasser, a SIL-20ACXR autosampler, and a CTO-20 AC column oven (Shimadzu Corp., Columbia, MD). A 2 μL sample was injected into a C18 column (2.0 μm, 2.1 × 150 mm, SHIMADZU) and the column oven was kept at 40 °C. The water with 0.1% formic acid (A) and acetonitrile (B) were used as the mobile phase at a flow rate of 0.4 mL/min with the following gradient profile: 0.0 min, 95% A; 2.0 min, 95% A; 9.0 min, 5% A; 11.5 min, 95% A; 12 min, 95% A; 15 min, 95% A.

Mass spectrometric analysis was achieved on a TripleTOF 5600$^+$ mass spectrometer (AB SCIEX, Redwood City, CA, USA), AB SCIEX Analyst TF v.1.6 software, and MS and MS/MS data acquired in negative ion modes from *m/z* 100 to 700. Source parameters were: gas 1, 50 psi; gas 2, 50 psi; curtain gas, 35 psi; temperature, 450 °C; ion spray voltage, 4.5 kV; declustering potential, 80 V.

2.14. PAMPA permeability study

Singh et al. have described the PAMPA method [24]. A 96-well filter plate pre-coated with lipids was used as the permeation acceptor and a 96-well receiver plate was used as the permeation donor. Stock solutions of the drug samples were prepared at a concentration of 10 mM in DMSO. The PAMPA plate was filled with 300 μL diluted drug solution to prepare the donor wells, and the 96-well filter plate containing a synthetic phospholipid membrane was then placed on the donor wells. The acceptor wells were filled with 200 μL buffer solution and the PAMPA instruments were incubated at room temperature for 5 h. Licoricidin permeability was assessed in quadruplicate at pH 4.0 and 7.4. Naproxen was used as the high-permeability marker and furosemide as the low-permeability marker. At the end of the incubation, the amounts of licoricidin and the marker compounds in the donor and acceptor wells were measured by HPLC and the permeability was calculated.

3. Results

3.1. Analysis of licoricidin metabolites by HPLC and LC-MS/MS

We first used HPLC to detect the quantity of metabolites. The mobile phases and chromatographic conditions are described in Section 2.3. After licoricidin (20 μM) was incubated with HLMs, MLMs, DLMs, PLMs, RLMs, or RAMs (0.3 mg protein/mL), we used HPLC to analyze the samples and we observed five new peaks (P_1–P_5). The new peaks were identified as licoricidin metabolites by comparison with the control group (CTRL) (Fig. 2). The formation of metabolites was time-, NADPH-, and microsome-dependent. The retention times (Rt) of the five metabolites from P_1 to P_5 were 8.88, 9.75, 11.53, 11.82, and 12.67 min, respectively. P_3 was the most important metabolite with the highest peak area. The P_3 peak areas for DLMs, RLMs, PLMs, RLMs, and RAMs were 45-, 59, 82-, 0.73-, and 9.13-fold that for HLMs. However, the licoricidin peak areas in DLMs, RLMs, PLMs, RLMs, and RAMs were 0.55-, 0.81-, 0.55-, 1.04-, and 0.84-fold that for HLMs. Therefore, we

Table 1
Mass spectral characterization of licoricidin and its metabolites in HLMs, MLMs, RAMs, RLMs, DLMs, and PLMs.

Number	Rt (min)	Formula	[M-H]⁻	Fragment	Error(ppm)	Metabolic reaction	Peak area (%)					
							Human	Dog	Monkey	Rabbits	Pigs	Rats
M_0	10.66	$C_{26}H_{32}O_5$	423.2174	391,233,207,203, 189,177,163,137	−0.7	Parent	52.6	46.87	36.94	45.1	31.05	36.9
M_1	8.21	$C_{26}H_{32}O_6$	439.2117	407,355,283,233,207	+1.8	Hydroxylation	0.96	5.25	1.28	1.73	6.37	7.53
M_2	7.88	$C_{26}H_{32}O_6$	439.2119	407,349,249,233,215,203,177	−1.2	Hydroxylation	0.25	1.59	0.89	1.05	0.83	1.23
M_3	9.21	$C_{26}H_{30}O_6$	437.1832	283,255,241,219,207	−1.1	Hydroxylation + dehydrogenation	ND	0.09	0.03	0.01	0.08	ND
M_4	8.14	$C_{26}H_{24}O_8$	455.2072	394,379,283,233.219,205	+1.6	2 × Hydroxylation	0.15	0.36	ND	0.33	0.59	0.92
M_5	10.24	$C_{26}H_{34}O_7$	457.1192	385,355,303,283,279,255,241,205	+1.3	2 × Hydroxylation + reduction	ND	0.06	ND	ND	0.06	0.06
M_6	9.76	$C_{26}H_{26}O_7$	441.2382	303,283,255,241	+0.2	Hydration	0.02	0.54	0.05	0.08	0.28	0.39
M_7	9.73	$C_{26}H_{34}O_7$	457.2355	355,329,311,303,283,279,255,241	−1.9	2 × Hydroxylation + reduction	ND	ND	ND	ND	0.07	ND

used LC-MS/MS to determine the structures of the metabolites. The mobile phases and chromatographic conditions are described in Sections 2.3 and 2.11. Based on the direct comparison with the mass spectra of the blank samples, the structures of seven metabolites were identified in all the samples. We detected four (M_1, M_2, M_4, and M_6), six (M_1–M_6), four (M_1–M_3 and M_6), five (M_1, M_2, and M_4–M_6), seven (M_1–M_7), and five (M_1–M_4 and M_6) licoricidin metabolites in HLMs, DLMs, MLMs, RLMs, PLMs, and RAMs, respectively. M_1 and M_2 were identified as hydroxylation products, and M_6 was identified as a hydration product of licoricidin. The LC-MS/MS data are summarized in Table 1, and the MS/MS spectra of licoricidin and its metabolites are displayed in the supplemental materials (Fig. S1). The structural analysis of metabolites was based on MS/MS information.

3.1.1. Parent compound

Licoricidin, with a formula of $C_{26}H_{32}O_5$ (*m/z* 423.2174), produced eight key fragment ions at *m/z* 391, 233, 207, 203, 189, 177, 163, and 137 (Fig. S1A). The fragment ion at *m/z* 391 was formed by the loss of two hydroxyl groups from the parent molecule, and produced a daughter ion at *m/z* 207 directly. Ring B of licoricidin underwent a ring-cross cleavage reaction and generated the product ion at *m/z* 233, which produced a series of fragment ions at *m/z* 219, 203, and 163. Cleavage of licoricidin at C-3 produced a daughter ion at *m/z* 231, which produced further fragment ions at *m/z* 215, 231, 177, and 137. In addition, we did not assign the structures of fragment ions at *m/z* 391 and 215.

3.1.2. M_1 and M_2

M_1 (Rt = 8.21 min) and M_2 (Rt = 7.88 min) were isomers with the same molecular formula of $C_{25}H_{24}O_7$ (*m/z* 439) and different Rt. Two metabolites had *m/z* of 16 Da more than licoricidin, indicating that they were hydroxylated products of licoricidin, but that the locations of the hydroxylation were different. According to exact mass determination and the corresponding chemical composition, M_2 and M_1 were produced through the addition of a hydroxyl group to the parent molecule on the phenyl ring and at C-4″, respectively (Figs. S1B and C).

3.1.3. M_3

The molecular formula of M_3 was determined as $C_{26}H_{30}O_6$ (*m/z* 437.1832) with five characteristic fragment ions at *m/z* 283, 255, 241, 219, and 207. The structural formula and fragmentation pathway of M_3 are shown in Fig. S1D. Hydroxyl groups and side chains in the *ortho* position are prone to cyclization [10,25]. The MS/MS spectra of M_3 indicated that M_3 was a cyclization product from the reaction of licoricidin at C-7-OH and C-4″, and the addition of a hydroxyl group at C-5′.

3.1.4. M_4 and M_5

M_4 and M_5 gave $[M-H]^-$ ions at *m/z* 455.2072 and 457.1192, and their fragment ions and fragmentation pathways are shown in Fig. S1E and F. M_4 had *m/z* of 16 Da more than M_1, suggesting that M_4 was the hydroxylated product of M_1. The MS/MS information proved that a hydroxyl group was added at C-5′ of M_1. M_5 had *m/z* of 2 Da more than M_4 and was identified as the reduction product of M_4, with two hydrogens added at C-2″ and C-3″.

3.1.5. M_6

The high-resolution mass spectrum of M_6 (Fig. S1G) established the molecular formula as $C_{26}H_{26}O_7$ (*m/z* 441.2382), indicating that it was a hydrated or hydrogenated then hydroxylated product of licoricidin. Characteristic fragment ions at *m/z* 283, 255, and 241 indicated that the hydration occurred at C-5′.

3.1.6. M_7

M_7 and M_5 were isomers with $[M-H]^-$ ions at *m/z* 457.2355. High-resolution mass spectra showed that M_7 was the reduction and double

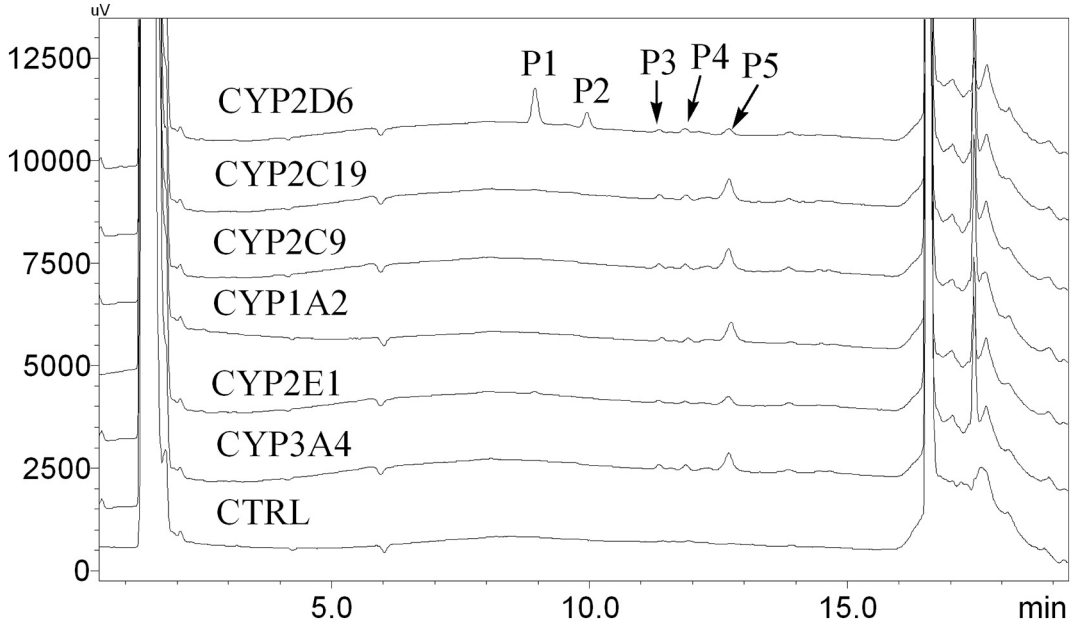

Fig. 3. Representative HPLC profiles of licoricidin and its metabolites in recombinant CYP supersomes. Licoricidin (20 μM) was incubated with recombinant CYP supersomes (15 nM) at 37 °C for 30 min.

hydroxylation product of licoricidin. The characteristic fragment ions at *m/z* 355 and 279 suggested one −OH was added at C-10′ (or C-11′) and the reduction reaction occurred at C-8′ and C-9′. The fragment ions at *m/z* 283, 255, and 241 indicated that the other −OH was added at C-5′ (Fig. S1H).

3.2. CYP isoforms involved in catalyzing the formation of metabolites

CYP1A2, CYP2C9, CYP2C19, CYP2D6, CYP2E1, and CYP3A4 are the main CYP isoforms involved in metabolizing many drugs. We incubated licoricidin with these cDNA-expressed human CYP isoforms to confirm the CYP isoforms involved in catalyzing licoricidin metabolite formation. Fig. 3 shows that all six CYP isoforms were involved in the formation of P_3, P_4, and P_5, and then only CYP2D6 catalyzed the formation of P_1 and P_2.

The chemical inhibition study also indicated which CYP isoforms were involved in the formation of metabolites. Licoricidin was incubated with selective chemical inhibitors of the six CYP isoforms in RLMs, and quinidine (a CYP2D6 inhibitor) substantially inhibited the formation of P_1 and P_2 compared with other CYP isoform inhibitors (Fig. S2). Each of the selective inhibitors for CYP1A2, CYP2C9, CYP2C19, CYP2D6, CYP2E1, and CYP3A4 showed weak effects on the formation of P_3–P_5.

3.3. Enzyme kinetics study

Kinetic parameter values (K_m, V_{max}, and CL_{int}) in DLMs, RLMs, PLMs, and HLMs were calculated using P_3 data. The metabolism profiles of licoricidin (1–200 μM) for the different species exhibited typical monophasic Michaelis-Menten kinetics, which were further confirmed by Eadie-Hofstee plots (Fig. 4). The reaction velocities showed major concentration-dependent characteristics. The kinetic parameters K_m, V_{max}, and CL_{int} are summarized in Table 2.

3.4. Prediction of in vivo hepatic clearance in rats

We used the kinetic parameters of P_3 generated from non-linear regression in HLMs, DLMs, and RLMs to calculate CL_H, and the results were 9.05, 13.41, and 19.63 mL/min/kg body weight for humans, dogs, and rats, respectively. The percentages of CL_H versus hepatic blood flow (Q_H) for humans, dogs, and rats were 43.7, 43.4, and 35.5%, respectively.

3.5. Inhibitory effects of licoricidin against UGT and CYP activities

At a concentration of 100 μM, licoricidin inhibited the activity of 4-MU glucuronidation by 100% (UGT1A3, UGT1A6, UGT1A7, UGT1A9, UGT2B4, UGT2B7, and UGT2B15), 21.71% (UGT1A1), 5.85% (UGT1A8), 86.81% (1A10), and 3.84% (UGT2B17). In addition, 100 μM licoricidin inhibited the activities of CYP2C9, CYP2C19, and CYP3A4 by > 90%. We determined the inhibition kinetic parameters of UGT1A7, UGT2B7, and CYP3A4. Licoricidin exhibited concentration-dependent inhibitory behavior against UGT1A7, UGT2B7, and CYP3A4, with IC_{50} values of 1.78, 2.75 and 9.83 μM, respectively (Figs. 5A, 6A, and 7A). Furthermore, the Lineweaver-Burk plots (Figs. 5B, 6B, and 7B) showed that licoricidin non-competitively inhibited UGT1A7 and UGT2B7, and competitively inhibited CYP3A4. The K_i values calculated by a second plot of the slopes from the Lineweaver-Burk plots versus licoricidin concentrations were 0.76, 0.78, and 8.91 μM for UGT1A7, UGT2B7, and CYP3A4, respectively.

3.6. Molecular modeling

CYP2D6 is an important metabolic enzyme catalyzing the biotransformation of licoricidin. Licoricidin showed a strong inhibitory effect against CYP3A4. We used molecular docking to confirm the interaction between licoricidin and CYP2D6 or CYP3A4 at a molecular level. Licoricidin bound to the active cavity of CYP2D6 through hydrogen bonding and π-π stacking interactions (Fig. 8A). The hydrogen bonds were with Asp301 and Ser304, and the π-π stacking interactions were with Phe120 and Phe483. The isopentyl side chain fitted into the hydrophobic cavity formed by Val370, Phe483, and Leu484. Licoricidin also bound to the active cavity of CYP3A4 through hydrogen bonding and π-π stacking interactions (Fig. 8B). The hydrogen bonds were with Arg106, Arg372, and Glu374, and the π-π stacking interactions were with Phe57. The isopentyl side chain fitted into the hydrophobic cavity formed by Phe213, Phe215, and Thr224.

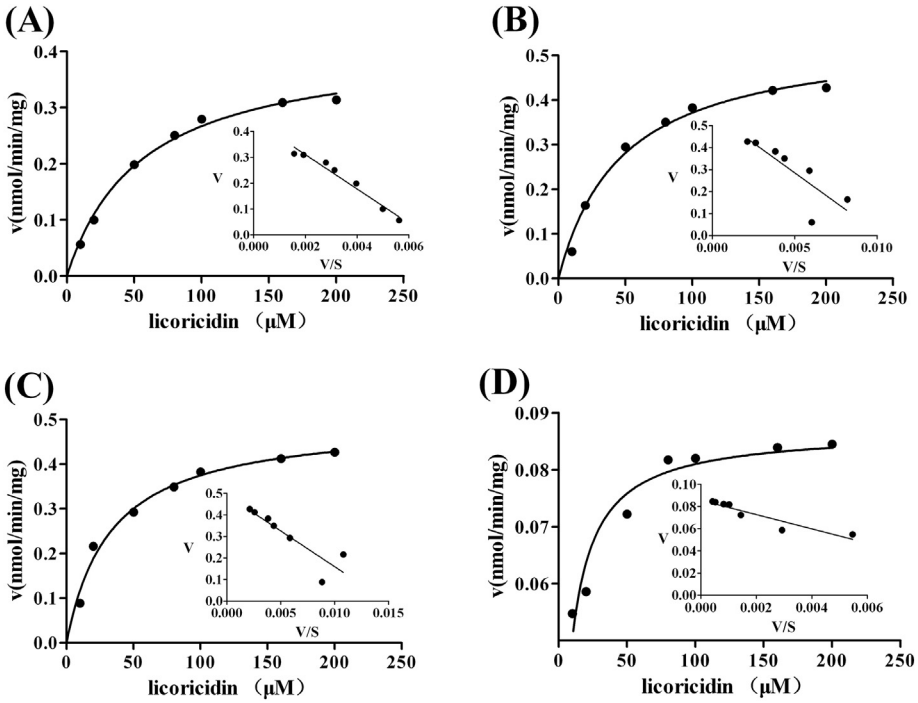

Fig. 4. Michaelis-Menten plots for licoricidin in DLMs (A), RLMs (B), PLMs (C), and HLMs (D). The corresponding Eadie-Hofstee plots were shown as insets. Each data point represents the mean of triplicate determinations.

Table 2
Kinetic parameters of P_3 production from licoricidin in pooled DLMs, RLMs, PLMs, and HLMs.

kinetic parameters	species			
	DLMs	RLMs	PLMs	HLMs
V_{max}(nmol/min/mg protein)	0.37 ± 0.02	0.47 ± 0.03	0.44 ± 0.02	0.09 ± 0.002
K_m (μM)	39.04 ± 6.49	27.26 ± 7.77	19.83 ± 5.13	7.33 ± 1.27
CL_{int}(mL/min/mg protein)	0.0095	0.017	0.022	0.012

3.7. Glucuronidation of licoricidin

The total ion and extracted ion chromatograms were showed in Figs. S3 and S4, and the MS/MS spectra of licoricidin and its glucuronidation metabolite were showed in Fig. S5. According to the total ion chromatograms, we found a new peak in 8.2 min as compared to the control group. The formation of the metabolite was UDPGA and microsome dependent. Extracted ion chromatograms showed that the metabolite gave $[M-H]^-$ ion at *m/z* 599.2455, and its main fragment ion was at *m/z* 423.2157.

3.8. PAMPA permeability of licoricidin

The PAMPA assay was carried out at both pH 4.0 and 7.4 because drug absorption occurs primarily in the small intestine, where the pH may vary from acidic to neutral or slightly basic [24]. Table 3 shows the PAMPA permeability results for licoricidin and the permeability markers. Licoricidin was a moderately permeable compound at pH 4.0 and 7.4.

4. Discussion

In the drug discovery process, it is important to assess the potential for new compounds to cause HDIs via inhibiting CYP- or UGT-dependent metabolism [26]. An initial study reported that licoricidin (10 μM) strongly inhibited CYP2B6, CYP2C8, CYP2C9, CYP2C19, and CYP3A4 [3]. A drug with an IC_{50} value of < 100 μM is considered to be potent inhibitor of CYP enzymes, which can lead to undesirable HDIs [27–29]. In this study, we found that 100 μM licoricidin strongly inhibited CYP2C9, CYP2C19, and CYP3A4, and almost all the UGT enzymes tested. The values of kinetic parameters IC_{50} and K_i for UGT1A7, UGT2B7, and CYP3A4 were all < 10 μM. K_i indicates the absolute affinity of an inhibitor for its target enzyme, and a lower K_i value means that the inhibitor has a stronger inhibitory effect on the target enzyme [30]. CYP3A4 is an important metabolic enzyme in the human liver,

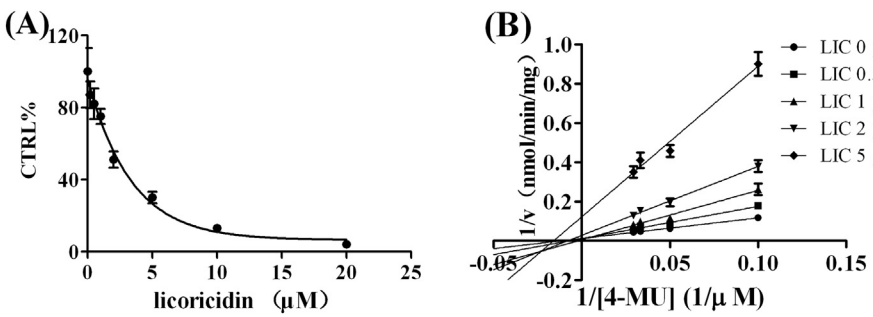

Fig. 5. Inhibition kinetic analysis of licoricidin (LIC) for recombinant UGT1A7-catalyzed 4-MU glucuronidation. (A) Licoricidin showed dose-dependent inhibition of UGT1A7. (B) Lineweaver-Burk plot of licoricidin inhibition of UGT1A7-catalyzed 4-MU glucuronidation. Every data point represents the mean of triplicate determinations.

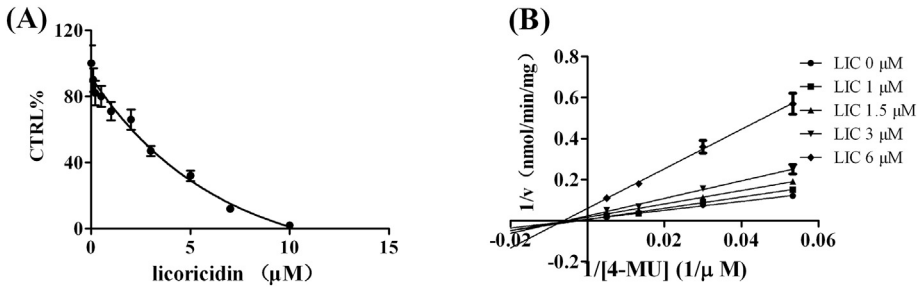

Fig. 6. Inhibition kinetic analysis of licoricidin (LIC) for recombinant UGT2B7-catalyzed 4-MU glucuronidation. (A) Licoricidin showed dose-dependent inhibition of UGT2B7. (B) Lineweaver-Burk plot of licoricidin inhibition of UGT2B7-catalyzed 4-MU glucuronidation. Every data point represents the mean of triplicate determinations.

and thus inhibition of CYP3A4 could result in HDIs and severe adverse side effects. Ibrutinib is a substrate for CYP3A4, and the metabolism of ibrutinib was inhibited by the CYP3A4 inhibitor, verapamil, which caused severe diarrhea in a patient when it was co-administered [31]. In a patient on stable atorvastatin therapy, the side effect of rhabdomyolysis was exacerbated by the moderate CYP3A4 inhibitor, fluconazole [32]. Potential HDIs should be monitored when licoricidin is co-administered with other medications because it is a strong inhibitor of CYPs and UGTs.

We identified five metabolite peaks (P_1-P_5) by HPLC after licoricidin was incubated with liver microsomes from different species. P_3 was the main metabolite in these liver microsomes. Substantial licoricidin metabolism occurred in DLMs, RLMs, and PLMs compared with the other liver microsomes; thus, the licoricidin metabolism exhibited large species differences. The differences in CYP or UGT isoforms are a major cause of the differences in drug metabolism among different species [14].

Wang et al. reported that the metabolite of licoricidin incubated with RLMs was a monohydroxylated derivative and the hydroxyl group was located at C-4″ of the isoprenyl group [33]. However, the structure and characteristics of the other metabolites were not reported. We found seven licoricidin metabolites by LC-MS/MS and they were primarily biotransformed through hydration, hydroxylation, reduction, and dehydrogenation reactions. Hydration and hydroxylation were the major metabolic transformations of licoricidin that were found in all species, and the hydroxylated metabolite was the major metabolite with the largest percentage of the peak area (%) among the species. As in other compounds, the hydroxyl group is readily added to the end of the side chain (C-4″) [34]. In addition, all licoricidin metabolites were found in PLMs, which was consistent with the HPLC-UV result that licoricidin metabolism was greatest in PLMs. Some metabolites have similar or stronger pharmacological or toxicological activities. For example, some metabolized flavonoids, such as baohuoside I, have high estrogen-like bioactivities in vitro [35].

Screening assays and chemical inhibition studies confirmed the CYPs that were involved in the metabolism of licoricidin and showed that CYP2D6 was the main hepatic isoform that catalyzed the formation of P_1 and P_2. The formation of the other metabolites, including P_3, P_4 and P_5, were catalyzed by CYP1A2, CYP2C9, CYP2C19, CYP2D6, CYP2E1, and CYP3A4. If licoricidin were to be co-administered with CYP2D6 inhibitors, such as imipramine, HDIs would be likely to occur.

There are substantial differences in CYPs among different species, which results in different drug metabolism across species [14,36]. The similar K_m values among different species reflect comparable binding affinities towards the metabolic site and indicate species similarities [20]. In this study, none of the experimental species had comparable K_m values for the formation of P_3. The K_m values in DLMs, RLMs, and PLMs were much higher than those in HLMs and all the differences were statistically significant (all $P < 0.01$). Thus, when studying licoricidin, we should consider the metabolic differences between species when using other animals as models. In addition, the percentage of CL_H versus Q_H for humans, dogs, and rats were calculated to be 43.7, 43.4, and 35.5%, respectively. Using the CL_H predicted from the in vitro data, compounds can be classified as high-clearance drugs (> 70% liver blood flow), low-clearance drugs (< 30% liver blood flow), and intermediate-clearance drugs [37]. Licoricidin was classified as an intermediate-clearance drug in humans, dogs, and pigs.

Molecular docking was performed in this study and showed that licoricidin interacted with CYP2D6 and CYP3A4 through hydrogen bonds and π-π stacking. Licoricidin bound to the active cavity of human CYP2D6 containing residues Asp301, Ser304, Phe120, and Phe483. Phe120 is a key amino acid residue for the selectivity and region specificity of substrate binding and catalysis in the catalytic site of CYP2D6 [38]. In addition, licoricidin binds to the active cavity of human CYP3A4 containing residues Arg106, Arg372, Glu374, and Phe57. Arg106, Arg372, Glu374, and Phe57 are important drug binding residues in CYP3A4, and HDI may occur at these residues [39].

UGTs are important biochemical factors in cellular defense and detoxification, which play an important rolein the metabolism of many clinical drugs or their phase I metabolites [40]. Based on structure of licoricidin and its UGT inhibition data, it is likely that glucuronidation also is an important pathway for licoricidin clearance. So the aspect of licoricidin metabolism was evaluated using microsomes supplemented with UDPGA. After metabolism of licoricidin by liver microsomes (UGT incubation system), an obvious product peak was observed (Fig. S3). According to LC-TOF-MS/MS data (Figs. S4 and S5), the metabolite had m/z of 176 Da more than licoricidin, indicating that it was glucuronidation product of licoricidin. However, licoricidin contains three phenolic hydroxyl groups, which of the hydroxyl groups is glucuronidated, it is necessary to be verified by NMR in future.

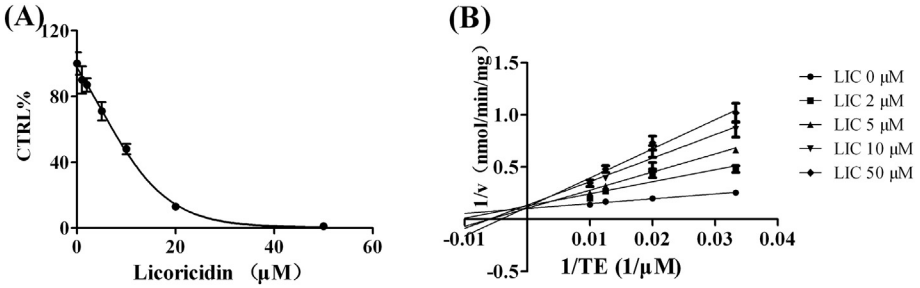

Fig. 7. (A) Inhibition of testosterone (TE) 6β-hydroxylation (CYP3A4) by licoricidin (LIC). (B) Lineweaver-Burk plot of inhibition of testosterone 6β-hydroxylation (CYP3A4) by licoricidin. Every data point represents the mean of triplicate determinations.

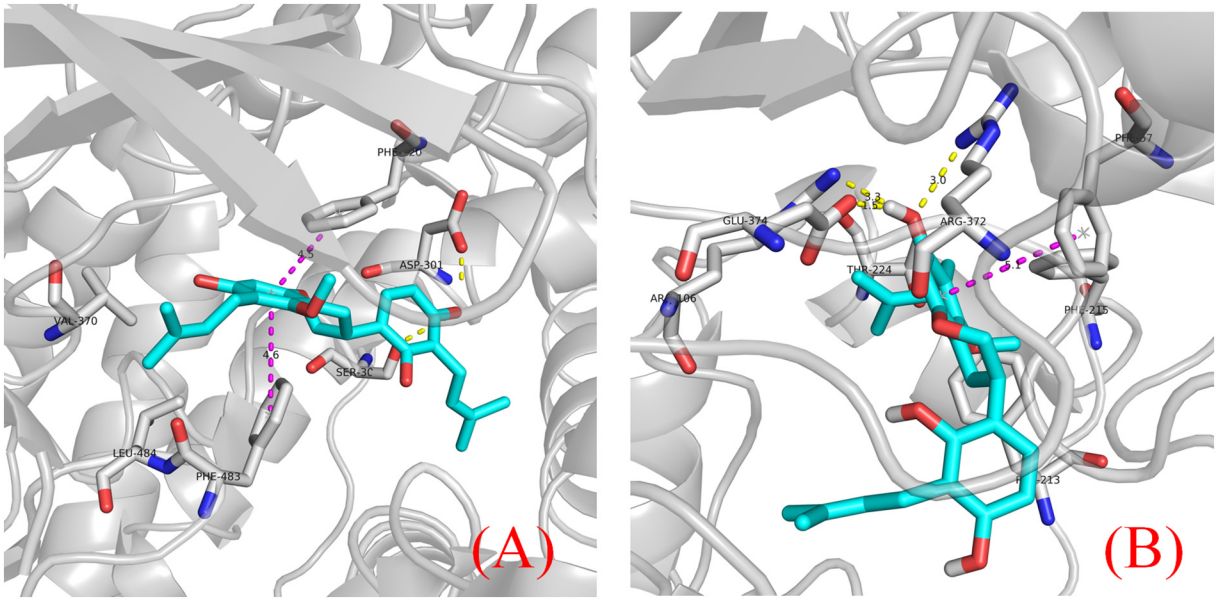

Fig. 8. Binding mode of licoricidin with (A) CYP2D6 and (B) CYP3A4. Licoricidin is shown in cyan, hydrogen bonds are displayed as yellow dotted lines, and π-π stacking is indicated by magenta dotted lines. (For interpretation of the references to colour in this figure legend, the reader is referred to the web version of this article.)

Table 3
PAMPA effective permeability (Pe) values of licoricidin and permeability markers.

Compound	Pe × 10^{-6} (cm/s)	
	PH = 4	PH = 7
Naproxen (high permeability marker)	6.28 ± 1.23	5.74 ± 1.54
Furosemide (low permeability marker)	0.03 ± 0.01	0.05 ± 0.01
Licoricidin	1.67 ± 0.36	2.92 ± 0.48

More than 80% of orally administered drugs are absorbed into the systemic circulation by passive diffusion through the intestinal epithelium. Hence, understanding the passive diffusion of a drug is useful for predicting the intestinal absorption and bioavailability [41]. PAMPA is used for high-throughput screening for passive transport [42]. In this study, we assessed licoricidin permeability at pH 4.0 and 7.4, which represents the conditions in the stomach, small intestine, and plasma. Licoricidin showed moderate permeability in acidic and slightly basic phases, indicating that licoricidin should be absorbed in the stomach and small intestine.

5. Conclusion

In conclusion, licoricidin exhibited potent inhibition against UGT1A3, UGT1A6, UGT1A7, UGT1A9, UGT2B4, UGT2B7, UGT2B15, CYP2C9, CYP2C19, and CYP3A4. Inhibition of these drug-metabolizing enzymes could lead to drug interactions; thus, our findings should stimulate clinical studies of drug interactions in patients receiving licoricidin. The metabolism of licoricidin showed substantial differences among species, and human possessed a lower metabolic capacity than other species. Many CYP isoforms (CYP1A2, CYP2C9, CYP2C19, CYP2D6, CYP2E1, and CYP3A4) were involved in licoricidin metabolism. LC-MS/MS spectra showed that hydration and hydroxylation were the major biotransformations of licoricidin, and the hydroxylated metabolite was the major metabolite. Molecular docking studies of the binding modes of licoricidin with CYP3A4 and CYP2D6 suggested that licoricidin interacted with CYP2D6 and CYP3A4 through hydrogen bonds and π-π stacking. Glucuronidation also is an important pathway for licoricidin clearance. The PAMPA permeability of licoricidin was moderate at pH 4.0 and 7.4.

Author contributions

Lina Shan, and Gang Zhang gave the idea, did the literature search, did the study, drafted the manuscript and statics analysis; Zhe Guo was the advisor and helped in the editing of the manuscript; Xianbao Shi was the supervisor and supervised the whole study. All authors read and approved the final version.

Declaration of Competing Interest

The authors declare that there is no conflict of interest.

Acknowledgements

The authors acknowledge financial support from the Doctoral Start-up Fund of Liaoning Province (Project no. 20170520140).

Appendix A. Supplementary data

Supplementary data to this article can be found online at https://doi.org/10.1016/j.lfs.2019.116770.

References

[1] J.E. Chaves, A. Melis, Biotechnology of cyanobacterial isoprene production, Appl. Microbiol. Biotechnol. 102 (2018) 6451–6458.
[2] H. Kirst, Y. Shen, E. Vamvaka, N. Betterle, D. Xu, U. Warek, J.A. Strickland, A. Melis, Downregulation of the CpSRP43 gene expression confers a truncated light-harvesting antenna (TLA) and enhances biomass and leaf-to-stem ratio in Nicotiana tabacum canopies, Planta 248 (2018) 139–154.
[3] G. Li, C. Simmler, L. Chen, D. Nikolic, S.N. Chen, G.F. Pauli, R.B. van Breemen, Cytochrome P450 inhibition by three licorice species and fourteen licorice constituents, Eur. J. Pharm. Sci. 109 (2017) 182–190.
[4] S.Y. Park, S.S. Lim, J.K. Kim, I.J. Kang, J.S. Kim, C. Lee, J. Kim, J.H. Park, Hexane-ethanol extract of Glycyrrhiza uralensis containing licoricidin inhibits the metastatic capacity of DU145 human prostate cancer cells, Br. J. Nutr. 104 (2010) 1272–1282.
[5] V.D. La, S. Tanabe, C. Bergeron, S. Gafner, D. Grenier, Modulation of matrix metalloproteinase and cytokine production by licorice isolates licoricidin and licorisoflavan A: potential therapeutic approach for periodontitis, J. Periodontol. 82 (2011) 122–128.
[6] S. Gafner, C. Bergeron, J.R. Villinski, M. Godejohann, P. Kessler, J.H. Cardellina, D. Ferreira, K. Feghali, D. Grenier, Isoflavonoids and coumarins from Glycyrrhiza uralensis: antibacterial activity against oral pathogens and conversion of isoflavans

into isoflavan-quinones during purification, J. Nat. Prod. 74 (2011) 2514–2519.
[7] S. Tanabe, J. Desjardins, C. Bergeron, S. Gafner, J.R. Villinski, D. Grenier, Reduction of bacterial volatile sulfur compound production by licoricidin and licorisoflavan A from licorice, J. Breath Res. 6 (2012) 016006.
[8] S. Ji, S. Tang, K. Li, Z. Li, W. Liang, X. Qiao, Q. Wang, S. Yu, M. Ye, Licoricidin inhibits the growth of SW480 human colorectal adenocarcinoma cells in vitro and in vivo by inducing cycle arrest, apoptosis and autophagy, Toxicol. Appl. Pharmacol. 326 (2017) 25–33.
[9] K.J. Kim, S.H. Xuan, S.N. Park, Licoricidin, an isoflavonoid isolated from Glycyrrhiza uralensis Fisher, prevents UVA-induced photoaging of human dermal fibroblasts, Int. J. Cosmet. Sci. 39 (2017) 133–140.
[10] X. Shi, G. Zhang, B. Mackie, S. Yang, J. Wang, L. Shan, Comparison of the in vitro metabolism of psoralidin among different species and characterization of its inhibitory effect against UDP- glucuronosyltransferase (UGT) or cytochrome p450 (CYP450) enzymes, J. Chromatogr. B Analyt. Technol. Biomed. Life Sci. 1029-1030 (2016) 145–156.
[11] S. Tang, A. Chen, X. Zhou, L. Zeng, M. Liu, X. Wang, Assessment of the inhibition risk of shikonin on cytochrome P450 via cocktail inhibition assay, Toxicol. Lett. 281 (2017) 74–83.
[12] U.M. Kent, M. Aviram, M. Rosenblat, P.F. Hollenberg, The licorice root derived isoflavan glabridin inhibits the activities of human cytochrome P450S 3A4, 2B6, and 2C9, Drug Metab. Dispos. 30 (2002) 709–715.
[13] A.A. Sprouse, R.B. van Breemen, Pharmacokinetic interactions between drugs and botanical dietary supplements, Drug Metab. Dispos. 44 (2016) 162–171.
[14] J. Zielinski, M. Mevissen, Inhibition of in vitro metabolism of testosterone in human, dog and horse liver microsomes to investigate species differences, Toxicol. in Vitro 29 (2015) 468–478.
[15] K. Sugano, Y. Nabuchi, M. Machida, Y. Asoh, Permeation characteristics of a hydrophilic basic compound across a bio-mimetic artificial membrane, Int. J. Pharm. 275 (2004) 271–278.
[16] M. Kansy, F. Senner, K. Gubernator, Physicochemical high throughput screening: parallel artificial membrane permeation assay in the description of passive absorption processes, J. Med. Chem. 41 (1998) 1007–1010.
[17] B.J. Bennion, N.A. Be, M.W. McNerney, V. Lao, E.M. Carlson, C.A. Valdez, M.A. Malfatti, H.A. Enright, T.H. Nguyen, F.C. Lightstone, T.S. Carpenter, Predicting a drug's membrane permeability: a computational model validated with in vitro permeability assay data, J. Phys. Chem. B 121 (2017) 5228–5237.
[18] P.K. Smith, R.I. Krohn, G.T. Hermanson, A.K. Mallia, F.H. Gartner, M.D. Provenzano, E.K. Fujimoto, N.M. Goeke, B.J. Olson, D.C. Klenk, Measurement of protein using bicinchoninic acid, Anal. Biochem. 150 (1985) 76–85.
[19] L.T. Nguyen, Z. Mysliveckova, B. Szotakova, A. Spicakova, K. Lnenickova, M. Ambroz, V. Kubicek, K. Krasulova, P. Anzenbacher, L. Skalova, The inhibitory effects of beta-caryophyllene, beta-caryophyllene oxide and alpha-humulene on the activities of the main drug-metabolizing enzymes in rat and human liver in vitro, Chem. Biol. Interact. 278 (2017) 123–128.
[20] Y.Y. Zhang, Y. Liu, J.W. Zhang, G.B. Ge, H.X. Liu, L.M. Wang, J. Sun, L. Yang, C-7 configuration as one of determinants in taxanes metabolism by human cytochrome P450 enzymes, Xenobiotica 39 (2009) 903–914.
[21] X. Shi, S. Yang, G. Zhang, Y. Song, D. Su, Y. Liu, F. Guo, L. Shan, J. Cai, The different metabolism of morusin in various species and its potent inhibition against UDP-glucuronosyltransferase (UGT) and cytochrome p450 (CYP450) enzymes, Xenobiotica 46 (2016) 467–476.
[22] Y. Naritomi, S. Terashita, S. Kimura, A. Suzuki, A. Kagayama, Y. Sugiyama, Prediction of human hepatic clearance from in vivo animal experiments and in vitro metabolic studies with liver microsomes from animals and humans, Drug Metab. Dispos. 29 (2001) 1316–1324.
[23] C. Formighieri, A. Melis, Cyanobacterial production of plant essential oils, Planta 248 (2018) 933–946.
[24] S.P. Singh, Wahajuddin, D. Tewari, K. Patel, G.K. Jain, Permeability determination and pharmacokinetic study of nobiletin in rat plasma and brain by validated high-performance liquid chromatography method, Fitoterapia 82 (2011) 1206–1214.
[25] W. Qu, X. Liu, Identification of cytochrome P450 isoforms involved in the metabolism of artocarpin and assessment of its drug-drug interaction, Biomed. Chromatogr. 32 (2018).
[26] J.Y. Lee, S.Y. Lee, S.J. Oh, K.H. Lee, Y.S. Jung, S.K. Kim, Assessment of drug-drug interactions caused by metabolism-dependent cytochrome P450 inhibition, Chem. Biol. Interact. 198 (2012) 49–56.
[27] Y. Pan, K.H. Tiong, B.A. Abd-Rashid, Z. Ismail, R. Ismail, J.W. Mak, C.E. Ong, In vitro effect of important herbal active constituents on human cytochrome P450 1A2 (CYP1A2) activity, Phytomedicine 21 (2014) 1645–1650.
[28] H. Rastogi, S. Jana, Evaluation of inhibitory effects of caffeic acid and quercetin on human liver cytochrome p450 activities, Phytother. Res. 28 (2014) 1873–1878.
[29] J. Savai, A. Varghese, N. Pandita, M. Chintamaneni, Investigation of CYP3A4 and CYP2D6 interactions of Withania somnifera and Centella asiatica in human liver microsomes, Phytother. Res. 29 (2015) 785–790.
[30] F.H. Darras, Y.P. Pang, On the use of the experimentally determined enzyme inhibition constant as a measure of absolute binding affinity, Biochem. Biophys. Res. Commun. 489 (2017) 451–454.
[31] K.E. Lambert, D. Leveque, B. Lioure, B. Gourieux, P. Bilbault, Adverse event potentially due to an interaction between ibrutinib and verapamil: a case report, J. Clin. Pharm. Ther. 41 (2016) 104–105.
[32] S.H. Hsiao, H.J. Chang, T.H. Hsieh, S.M. Kao, P.Y. Yeh, T.J. Wu, Rhabdomyolysis caused by the moderate CYP3A4 inhibitor fluconazole in a patient on stable atorvastatin therapy: a case report and literature review, J. Clin. Pharm. Ther. 41 (2016) 575–578.
[33] Q. Wang, Y. Qian, Q. Wang, Y.F. Yang, S. Ji, W. Song, X. Qiao, D.A. Guo, H. Liang, M. Ye, Metabolites identification of bioactive licorice compounds in rats, J. Pharm. Biomed. Anal. 115 (2015) 515–522.
[34] Q. Wang, X. Qiao, C.F. Liu, S. Ji, L.M. Feng, Y. Qian, D.A. Guo, M. Ye, Metabolites identification of glycycoumarin, a major bioactive coumarin from licorice in rats, J. Pharm. Biomed. Anal. 98 (2014) 287–295.
[35] Y.M. Hu, Y.T. Wang, S.C. Sze, K.W. Tsang, H.K. Wong, Q. Liu, L.D. Zhong, Y. Tong, Identification of the major chemical constituents and their metabolites in rat plasma and various organs after oral administration of effective Erxian Decoction (EXD) fraction by liquid chromatography-mass spectrometry, Biomed. Chromatogr. 24 (2010) 479–489.
[36] M. Stamou, X. Wu, I. Kania-Korwel, H.J. Lehmler, P.J. Lein, Cytochrome p450 mRNA expression in the rodent brain: species-, sex-, and region-dependent differences, Drug Metab. Dispos. 42 (2014) 239–244.
[37] X.Q. Li, A. Bjorkman, T.B. Andersson, L.L. Gustafsson, C.M. Masimirembwa, Identification of human cytochrome P(450)s that metabolise anti-parasitic drugs and predictions of in vivo drug hepatic clearance from in vitro data, Eur. J. Clin. Pharmacol. 59 (2003) 429–442.
[38] X. Zhou, Y. Wang, P.M. Or, D.C. Wan, Y.W. Kwan, J.H. Yeung, Molecular docking and enzyme kinetic studies of dihydrotanshinone on metabolism of a model CYP2D6 probe substrate in human liver microsomes, Phytomedicine 19 (2012) 648–657.
[39] M. Jayakanthan, S. Chandrasekar, J. Muthukumaran, P.P. Mathur, Analysis of CYP3A4-HIV-1 protease drugs interactions by computational methods for highly active antiretroviral therapy in HIV/AIDS, J. Mol. Graph. Model. 28 (2010) 455–463.
[40] Y.F. Cao, R.R. He, J. Cao, J.X. Chen, T. Huang, Y. Liu, Drug-drug interactions potential of icariin and its intestinal metabolites via inhibition of intestinal UDP-glucuronosyltransferases, Evid. Based Complement. Alternat. Med. 2012 (2012) 395912.
[41] W.M. Kong, Z. Chik, Z. Mohamed, M.A. Alshawsh, Physicochemical characterization of Mitragyna speciosa alkaloid extract and Mitragynine using in vitro high throughput assays, Comb. Chem. High Throughput Screen. 20 (2017) 796–803.
[42] Y. Wang, M.S. Chow, Z. Zuo, Mechanistic analysis of pH-dependent solubility and trans-membrane permeability of amphoteric compounds: application to sildenafil, Int. J. Pharm. 352 (2008) 217–224.